J. Ocean Univ. China (Oceanic and Coastal Sea Research)
https://doi.org/10.1007/s11802-023-5340-z
ISSN 1672-5182, 2023 22 (3): 683-696
http://www.ouc.edu.cn/xbywb/
E-mail:xbywb@ouc.edu.cn

Wave Azimuth Cutoff Compensation Method and the Multisatellite Networking Mode of SAR

WAN Yong[1), *], CUI Kun[1)], QU Ruozhao[2)], DAI Yongshou[1)], LI Ligang[1)], QU Xiaojun[1)], and ZHANG Xiaoyu[1)]

1) *College of Oceanography and Space Informatics*, *China University of Petroleum*, *Qingdao* 266580, *China*
2) *China College of Control Science and Engineering*, *China University of Petroleum*, *Qingdao* 266580, *China*

(Received January 24, 2022; revised May 12, 2022; accepted June 10, 2022)

Abstract Synthetic aperture radars (SARs) encounter the azimuth cutoff problem when observing sea waves. Consequently, SARs can only capture the waves with wavelengths larger than the cutoff wavelength and lose the information of waves with smaller wavelengths. To increase the accuracy of SAR wave observations, this paper investigates an azimuth cutoff compensation method based on the simulated multiview SAR wave synchronization data obtained by the collaborative observation *via* networked satellites. Based on the simulated data and the equivalent multiview measured data from Sentinel-1 virtual networking, the method is verified and the cutoff wavelengths decrease by 16.40% and 14.00%. The biases of the inversion significant wave height with true values decrease by 0.04 m and 0.14 m, and the biases of the mean wave period decrease by 0.17 s and 0.22 s, respectively. These results demonstrate the effectiveness of the azimuth cutoff compensation method. Based on the azimuth cutoff compensation method, the multisatellite SAR networking mode for wave observations are discussed. The highest compensation effect is obtained when the combination of azimuth angle is (95°, 115°, 135°), the orbital intersection angle is (50°, 50°), and three or four satellites are used. The study of the multisatellite networking mode in this paper can provide valuable references for the compensation of azimuth cutoff and the observation of waves by a multisatellite network.

Key words synthetic aperture radar (SAR); compensation effect; cutoff wavelength; multisatellite networking mode

1 Introduction

Sea waves are one of the most important ocean dynamic processes, including wind waves and swells. Wind waves are waves caused directly by local winds; swells are waves that leave the wind zone and act directly on the sea, or waves that pass out of the wind zone with steep reductions in wind speeds or sudden changes in wind directions. The study of wave generation and evolution mechanisms to clarify their internal structure and external characteristics, has become an important research field in physical oceanography, which is of significance for national defense, shipping, shipbuilding, ports and construction of offshore oil platforms. In addition, the study of global wave distribution can provide valuable information regarding the global climate change and ocean shipping. The current techniques to obtain wave parameters mainly include wave buoy observations, wave numerical model forecasts, and remote sensing observations. Wave buoy observation is currently recognized as the most accurate method to obtain wave parameters; however, buoys cannot be used to measure the sea state changes over a large spatial scale. In addition, the cost of buoys is relatively high, the maintenance of buoys is challenging after deployment, and the buoy involve several limitations associated with natural and social factors, which makes it challenging to perform long-term large-scale monitoring. Therefore, buoys are not the ideal means to obtain large-scale spatial wave observations. With the development of ocean technology, numerical wave prediction models have emerged, which can help acquire the wave parameters over a large spatial domain. However, the model result is based on the numerical calculation, and the forecast accuracy is limited by many factors, such as the accuracy of the driving wind field, setting of the initial conditions, and influence of the water depth. Thus, the accuracy of the model simulation is highly limited. Consequently, the wave model is not an ideal approach for wave information acquisition. The development of microwave remote sensing technology has provided a novel tool for the wave observation. Spectrometer, altimeters, and synthetic aperture radar (SAR) all can achieve a large range of wave observations. At present, the reported results correspond to those from field observations, and these methods are widely implemented in wave researches. The spectrometer can detect sea state information in a large range, and the accurate wave parameters can be calculated from the radar data by using the wave parameter inversion methods.

* Corresponding author. E-mail: wanyong@upc.edu.cn

However, due to the limitation of the working principle, the spatial resolution of the spectrometer is not high. The altimeter inverts the wave parameters through the waveform, which is easily polluted by the nearshore terrestrial electromagnetic environment, resulting in the low inversion accuracy of near-shore wave parameters, so that the accurate wave parameters cannot be obtained. SARs are satellite-based sensors that can provide two-dimensional information of waves independently of the weather and light conditions. Moreover, the spatial resolution of SARs is considerably higher than those of various other wave acquisition methods. The two-dimensional images of the sea surface obtained by using SARs can be inverted to the two-dimensional directional spectrum of waves. In addition, the wave spectrum can be obtained, and the significant wave height, mean wave period, wave propagation direction and other important wave parameters can be calculated. SARs thus represent a promising tool to obtain large-scale wave observations. The application of such sensors is of significance for examining the changing characteristics of global sea conditions (waves and wind fields), preventing disasters and mitigating marine disasters (giant waves and typhoons).

Based on the current researches, single-satellite SAR observations of waves involve a critical limitation, that is the phenomenon of azimuth cutoff. Due to the effect of velocity bunching, the moving sea surface leads to an additional Doppler shift. The SAR can only observe the waves with wavelengths larger than a certain value (swells, mainly) and cannot observe the comprehensive wave information. The problem of azimuth cutoff wavelengths critically limits the development of SAR operational observations of ocean waves and prevents the full use of rich SAR global ocean wave observation information, which hinders the application of SAR for global sea state and climate change monitoring.

Since 1991, considerable researches have been conducted in the field of wave observations by using SAR satellites, and a series of methods for the inversion of wave parameters from SAR wave spectra have emerged. Hasselmann and Hasselmann (1991) obtained the nonlinear transformation relation of the SAR image spectrum to the wave direction spectrum and developed the Max-Planck Institute (MPI) algorithm for the inversion of the wave direction spectrum from the SAR image spectrum. Mastenbroek and de Valk (2000) proposed a semiparametric method for wave spectrum inversion (SPRA), in which the first guess spectrum was not the wave spectrum obtained from a certain model but the wind and wave spectrum estimated from the wind vector information observed by the ERS scatterometer. Engen and Johnsen (1995) proposed an algorithm to obtain the cross-spectrum from SAR complex data. The algorithm represented an improved technique for the inversion of the wave direction spectrum from SAR images. This method could simultaneously resolve the ambiguity of 180° in the wave propagation direction and reduce the speckle noise. To overcome the shortcomings of MPI and SPRA, Sun (2005) proposed an improved wave spectrum inversion model, namely, the parameterized first guess spectrum model, and the optimal SAR spectrum obtained was consistent with the SAR image spectrum. Schulz-Stellenfleth *et al.* (2005) presented an empirical algorithm for wave parameters, known as used in Chinese WAVE database (CWAVE), which directly extracted the wave parameters from the ERS-2 SAR wave pattern data without determining the wave spectrum. The algorithm yielded satisfactory inversion results under low and medium sea state conditions, but the significant wave heights obtained from the inversion under high sea state conditions exhibited relatively large negative deviations. In addition, the author proposed a partition rescale and shift algorithm (PARSA), which is an extended and improved form of the MPI model and a combination product of the MPI model and cross-spectrum algorithm. The method can solve the problem of 180° ambiguity in the wave propagation direction and is more accurate than the cross-spectrum method; however, the method inherits the shortcomings of the MPI algorithm and requires the support of the initial guess wave spectrum and wave patterns. Schuler *et al.* (2004) developed a new technique to measure wave slopes in SAR azimuths and range directions. He (1999) derived the linear polarization directional modulation transfer function and tilt modulation transfer function, examined the effects of radar and wave parameters on the linearly polarized SAR image spectrum by numerically simulating the modulation transfer function, and proposed a method to eliminate the 180° direction ambiguity. Li (2010) extended and improved the empirical algorithm and proposed the CWAVE_ENV empirical model to be applied to ENVISAT ASAR wave pattern data. Moreover, the author evaluated the inversion results for high and low sea state conditions, and the accuracy was noted to be satisfactory. Bruck and Lehner (2012) developed an empirical algorithm, XWAVE, for the inversion of wave parameters for high-resolution Terra-SAR-X and Tandem-X data, and validated the sea state parameters by using buoy data obtained at the same location. The wave directions were validated by using the results of wave patterns, and the 2D wave spectra were validated according to the results of ocean radar Wamos; all the results indicated a reasonable agreement. Romeiser *et al.* (2015) proposed a new technique for extracting wave parameters based on C-band ScanSAR images, which determined the peak wavelength and direction from the image spectrum and estimated the significant wave height from the local average image intensity by using an empirical method. Using RADARSAT-2 fine single-polarization SAR data, Ren *et al.* (2015) proposed an empirical relationship between the significant wave height and SAR azimuth cutoff wavelength, which could be used to obtain the accurate significant wave height by the inversion at HH polarization. Zhang (2017) proposed a semiempirical algorithm for the inversion of the significant wave height and mean wave period based on SAR images of Sentinel-1 with C-band VV polarization. The semiempirical algorithm described the empirical relationships among the significant wave height and cutoff wavelength, radar incidence angle, and angle between the wave propagation direction and radar range direction. The results indicated that this semiempirical algorithm can per-

form the inversion of wave parameters of SAR images of Sentinel-1. Lin *et al.* (2017) proposed an empirical algorithm of CSAR_WAVE_S based on the cutoff wavelength inversion of the significant wave height and applied it to reali- ze the significant wave height inversion of HH polarized SAR images. The authors compared the results with NDBC buoy data and declared that the approach could realize significant wave height inversion without additional information. For the first time, Zheng *et al.* (2020) created the first wave climate dataset for the Maritime Silk Road in 2020. This creative research will make positive contribution to the disaster reduction. Notably, these studies were mainly related to the inversion of wave parameters of the wave spectrum.

After many years of technological development, several domestic and international scholars have conducted studies on the problem of the wave cutoff wavelength for SAR observations. Vachon *et al.* (1994) indicated that the distance-to-velocity ratio R/V is the key parameter to generate azimuth cutoff, and a larger R/V means that the SAR image spectrum is more sensitive to the azimuth cutoff and imaging nonlinearities. Kerbaol *et al.* (1996) proposed that the azimuth cutoff is the function of the wind speed and significant wave height. Hasselmann *et al.* (1985) analyzed the relationship between the cutoff wave-length and modulation transfer function (MTF). Marghany *et al.* (2002) applied the quasi-linear transformation method to estimate the significant wave height by using the cutoff wavelength based on the image data acquired by ERS-1. Ren *et al.* (2016) proposed a method to retrieve directional ocean wave spectra from SAR and wave spectrometer data. Stopa *et al.* (2015) used Envisat ASAR wave pattern data and buoy data to establish the relationship between the azimuth cutoff wavelength and wave orbit velocity. Grieco *et al.* (2016) used ESA Sentinel-1 data to study the relationship among the cutoff wavelength, wind speed and significant wave height and compare the results of the geophysical model function with the buoy data provided by NDBC; a root mean square error of approximately 0.5 m was observed. Corcione *et al.* (2018) proposed a method for the inversion of the wave wind speed based on the azimuth cutoff from the obtained SAR images. Li *et al.* (2019) analyzed the dependence of the azimuth cutoff on the polarization mode and incidence angle based on polarized Radarsat-2 and HMS-3 products. Most of these studies were focused on the mutual estimation of the cutoff wavelength and significant wave height, wind speed and other parameters, and the research regarding the elimination of the effect of azimuth cutoff and the compensation of the cutoff wavelength remains limited. Notably, Lyzenga and Malinas (1996) corrected the azimuth cutoff by dual-antenna SAR measurement of the wave spectrum and suggested that the effect of the cutoff wavelength could be compensated by using two SAR satellites in the future. This framework can be regarded as a prototype for the cutoff wavelength compensation.

At present, the problem of azimuth cutoff for SAR wave observations cannot be solved by using a single SAR satellite. The technology of small satellite networking has gradually developed in recent years, and it represents the future development trend of satellite observations to the Earth. In this context, the simultaneous observation of the same wave system from multiple viewpoints through small satellite SAR network might solve the problem of azimuth wavelength cutoff of SAR wave observation to a certain extent by using complementary information. However, it is necessary to identify the methods to compensate for the cutoff wavelength by the information obtained from the multisatellite network and the networking mode to be used for small satellite SARs to achieve the optimal compensation effect. Considering these aspects, this paper investigates a cutoff wavelength compensation technology based on the simulated multiview SAR wave synchronization data. Moreover, the small satellite SAR networking mode for wave observations is examined to determine the optimal orbital intersection angle, azimuth angle and number of satellites to achieve the optimal compensation effect and promote the application of SAR satellite networking.

2 Datasets and Methods

2.1 Multiview SAR Wave Synchronization Datasets

Before establishing the SAR wave cutoff wavelength compensation technique, it is necessary to prepare the simultaneous multiview wave observation data, *i.e.*, synchronized observation data of SARs in different flight directions for the same sea area. In this paper, we use the SAR imaging simulation technology to obtain the simulated observation data from different orbiting SAR satellites for different sea state waves as the multiview SAR wave synchronization data, which are subsequently used for the modeling and validation of the azimuth cutoff compensation method. The multiview SAR wave synchronization observation data are acquired by performing five steps: wave spectrum simulation, sea surface simulation, SAR echo simulation, SAR imaging simulation and generation of multiview SAR wave synchronization data (Wan *et al.*, 2019). The process of acquiring the multiview SAR wave synchronization observation data is shown in Fig.1.

The wave spectrum is the power density spectrum of the sea surface and reflects the statistical distribution of the wave energy in terms of the wavelength and propagation direction. In this paper, the two-dimensional PM wavenumber spectrum is used to simulate the wave spectrum, and the simulation of the wave spectrum is the basis of the sea surface simulation (He *et al*., 2004). The sea surface simulation provides the background field for the SAR echo simulation. After the sea surface is constructed, the radar emits electromagnetic waves to the sea surface and receives their echoes, and the analysis of the echoes can yield the original echo data. Therefore, the simulation construction of the sea surface scene is the basis for the echo simulation. This paper adopts the Monte Carlo method to simulate the sea surface (Mao *et al*., 2013; Xu *et al*., 2013). After the sea surface simulation, the echo signal model must be established. Two aspects of the simulation of sea

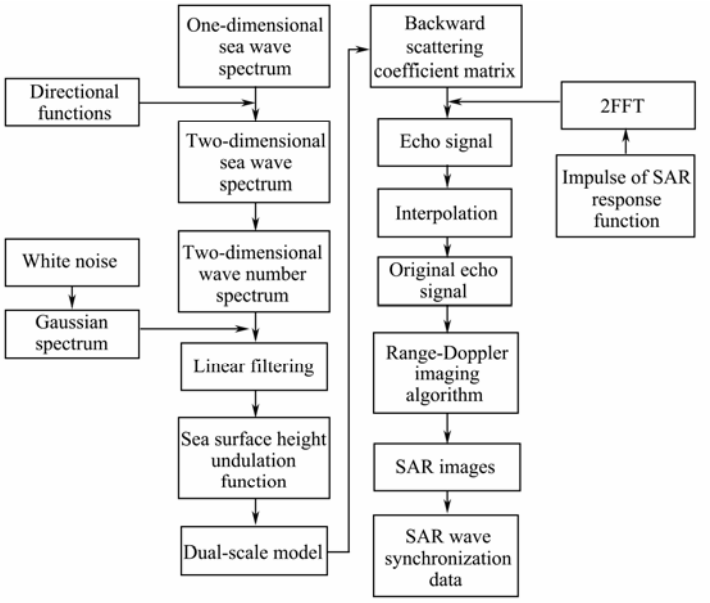

Fig.1 Flow chart of multiview SAR wave synchronization data acquisition.

surface echo data must be examined specifically: obtaining the sea surface backward scattering coefficients, and simulating the original sea surface SAR echo data. In this paper, a dual-scale electromagnetic scattering model is used to calculate the sea surface backward scattering coefficients (Guo, 2011) and subsequently a time-domain echo algorithm is applied to generate the raw echo data, which can be interpolated to obtain the echo data required for imaging (Huang, 2008). In the SAR imaging processing, the two-dimensional distribution of the target backward scattering coefficients is extracted from the echo data. This procedure pertains to two-dimensional correlation processing. According to the working principle of the SAR system, the echo data are obtained from the simulation of the height coefficients at the sea surface, and SAR images are later obtained by the Range-Doppler imaging algorithm (Alpers, 1985; Pi *et al*., 2007). The simulation of synchronous data is the last step for the multiview SAR wave synchronous data acquisition. After the single-satellite SAR wave data are obtained by the imaging algorithm, this SAR satellite is used as the reference satellite. Ignoring the ground curvature and rotation of the Earth, the sea wave observation data of the SAR satellites under different flight directions from the reference SAR satellite are simulated and obtained.

Finally, we obtained 19 sets of multiview SAR wave synchronization data with the azimuth angle from 0° to 180° at 10° intervals based on the imaging simulation techniques. The basic SAR system parameters are set as 530 km for platform height, 7600 $m s^{-1}$ for platform speed and 30° for angle of incidence. The wave propagation direction is set as 45° and the wind speed as 10 $m s^{-1}$ at a height of 10 m above the sea surface.

2.2 Multisatellite Wave Spectrum Data Fusion and Cutoff Wavelength Compensation

Azimuth cutoff is a measure of the capability of SAR in azimuth observations. Due to the nonlinear influence of velocity bunching effect, the azimuth cutoff occurs in the SAR observation of waves. Velocity bunching modulation can disrupt the coherence of SAR echoes, resulting in the Doppler shift in the azimuth direction. If the ratio of the displacement to the longwave wavelength on the SAR image is not large, the effect of displacement is linear, and if the displacement is greater than or equal to the wave-length, the effect is non-linear.

The wave spectrum observed by using a single satellite SAR has incomplete information, owing to the problem of cutoff wavelength in azimuth direction. The information of multiple observation directions can be obtained when the same sea area is observed by a group of SAR satellites, and the corresponding observation mode is schematically shown in Fig.2. The wave spectrum observed by each satellite in the multisatellite network carries the information pertaining to different directions, which can compensate each other, thereby reducing the effect of the cutoff wavelength to a certain extent. In this paper, we use a cutoff wavelength compensation method based on the wave spectral level information fusion, which extracts the wave spectra of each single satellite using the MPI method and accomplishes cutoff wavelength compensation by fusing the wave spectra obtained from the inversion of multiview SAR wave synchronization data (Wan *et al*., 2020a).

To compensate for the cutoff wavelength, the determination of the fusion weights for the wave spectrum of each satellite is of significance. Since the wave spectra of each satellite are not completely independent, the fusion weights must be determined considering that the sum of the weights is less than one. In the paper, azimuth angle is defined as the angle between the direction of wave propagation and the direction of SAR flight. Wan *et al.* (2020b) studied the effect of azimuth angle on the cutoff wavelength and found that in the acute angle range, the cutoff wavelength increases with the increase of the azimuth angle; in the ob-

tuse angle range, as the azimuth angle increases, the cutoff wavelength decreases. According to the relationship between the azimuth angle and the cutoff wavelength, in this paper, azimuth angle is defined as the angle between the direction of wave propagation and the direction of SAR flight, and the method of determining the weights in quadrants can be described as follows:

1) When the sum of the azimuth angles lies in the range of 0°–90°, the weight is determined as the ratio of the azimuth angle to 90°; when the azimuth angles are acute, the cutoff wavelength increases with the azimuth angle.

2) When the sum of the azimuth angles lies in the range of 90°–180°, and if the cutoff wavelength increases with the azimuth angle, the weight is determined as the ratio of the azimuth angle to 180°.

3) When the sum of azimuth angles lies in the range of 180°–270°, and if the cutoff wavelength decreases with increasing azimuth angle, the weight is set as the ratio of the inverse order of each azimuth angle to 270° according to the inverse distance weighting principle.

4) When the sum of the azimuth angles lies in the range of 270°–360°, the correction weight is determined as the ratio of the inverse order of each azimuth angle to 360°; in this case, the azimuth angles are obtuse, and the cutoff wavelength decreases with increasing azimuth angle.

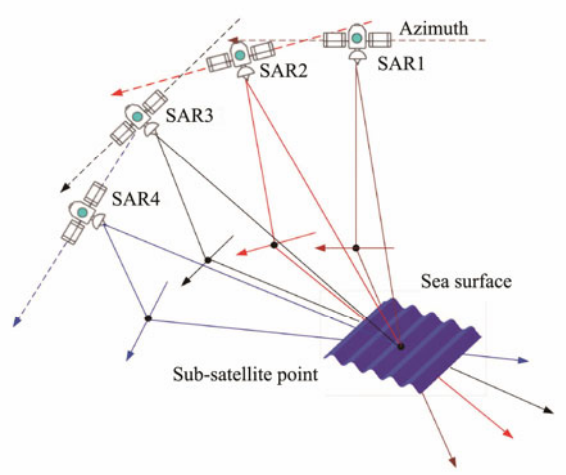

Fig.2 SAR network cooperation to observe the same sea area.

After the fusion weights are determined, the wave spectra are fused according to the established information fusion method. The optimal wave spectra to be fused are multiplied by the corresponding fusion weights, and the summed results represent the fused optimal wave spectra. Wave spectrum fusion is the process of fusing the energy information of each independent wave spectrum to form a wave spectrum with complete energy information. For example, for a three-satellite network, when the sum of the azimuth angles lies between 0° and 90°, 90° and 180°, 180° and 270°, and 270° and 360°, the spectral fusion equations are given in Eqs. (1)–(4).

$$WS=\frac{\theta_1}{90}WS_1+\frac{\theta_2}{90}WS_2+\frac{\theta_3}{90}WS_3, \tag{1}$$

$$WS=\frac{\theta_1}{180}WS_1+\frac{\theta_2}{180}WS_2+\frac{\theta_3}{180}WS_3, \tag{2}$$

$$WS=\frac{\theta_3}{270}WS_1+\frac{\theta_2}{270}WS_2+\frac{\theta_1}{270}WS_3, \tag{3}$$

$$WS=\frac{\theta_3}{360}WS_1+\frac{\theta_2}{360}WS_2+\frac{\theta_1}{360}WS_3, \tag{4}$$

where WS_1, WS_2 and WS_3 represent the wave spectra from SAR data of each satellite, θ_1, θ_2 and θ_3 represent the azimuth angles corresponding to the wave spectra WS_1, WS_2 and WS_3, respectively, and WS represents the wave spectrum after data fusion.

The cutoff wavelength compensation method used in this paper is a method based on the abovementioned fusion calculation of the spectral information. This approach ensures that the cutoff wavelength after fusion is smaller than the initial cutoff wavelength to reduce the influence of the cutoff wavelength to a certain extent.

3 Results and Discussion

3.1 Simulation Data-Based Validation

After establishing the cutoff wavelength compensation method for wave spectrum information fusion, the compensation effect must be verified. An example of a three-satellite network with the set of azimuth angles being 35°, 45° and 55° and simulation data are used to verify the effect of the cutoff wavelength compensation method. The fusion is performed as Eq. (5):

$$WS=\frac{35}{180}WS_1+\frac{45}{180}WS_2+\frac{55}{180}WS_3. \tag{5}$$

In the paper, we use the MPI method to obtain the wave spectra. In the process of inversion of wave spectra and SAR image spectra by the MPI method, the SAR image spectrum and the initial guess spectrum–E spectrum are input firstly, and the simulated SAR spectrum is calculated from the initial guess spectrum by forward mapping. Then, the simulated SAR spectrum and the observed SAR image spectrum are used to calculate the cost function, and the cost function is used to judge whether the iterative process converges. When the value function is the smallest, the wave spectrum obtained by inversion is closest to the initial guess spectrum, and the optimal wave spectrum and optimal SAR spectrum are obtained at this time.

The results of the wave spectra before and after the information fusion are shown in Fig.3.

The effectiveness of the cutoff wavelength compensation method is verified by comparing the cutoff wavelengths, significant wave heights, and mean wave periods before and after the wave spectrum fusion. To evaluate the accuracy of the wave parameter inversion, it is necessary to provide the true significant wave height, which is estimated here by the wind speed according to the Eq. (6):

$$H_s=0.0214\cdot U_{19.5}^2, \tag{6}$$

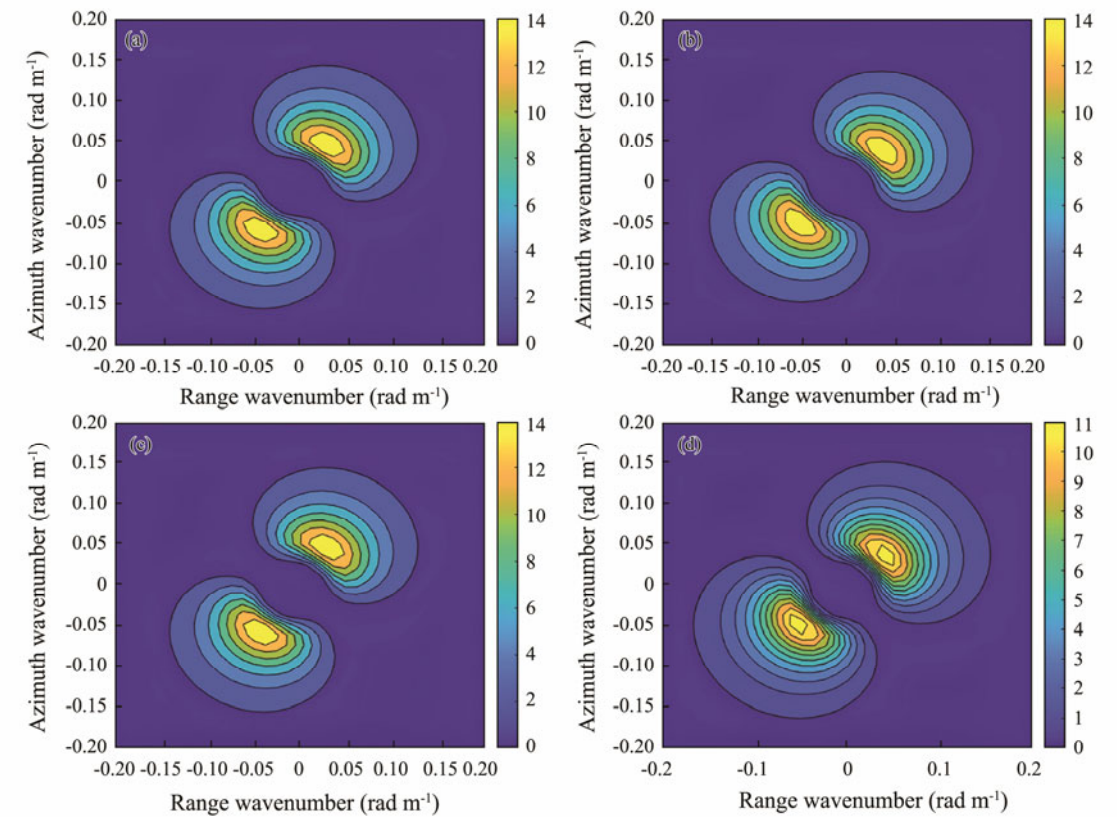

Fig.3 Results of wave spectra from different azimuths before and after fusion. (a), 35°; (b), 45°; (c), 55°; (d), fusion of the wave spectrum.

where $U_{19.5}$ represents the wind speed at the height of 19.5 m above sea level, which is converted from the wind speed at the height of 10 m above sea level U_{10}, often used in the wave calculations, according to Eq. (7):

$$U_h = U_{10} \cdot \left(1 + 2.5 \lg\left(\frac{h}{10}\right)\right) \cdot \left(\sqrt{0.0015 / \left[1 + \exp\left(-\frac{U_{10} - 1.25}{1.56}\right)\right]} + 0.00104\right). \quad (7)$$

The significant wave height and mean wave period are obtained by inversion using the MPI method, and the significant wave height is calculated as Eq. (8):

$$H_s = 4\sqrt{m_0} = 4\sqrt{\int_0^\infty \int_0^\infty S(k_x, k_y) \mathrm{d}k_x \mathrm{d}k_y}\ . \quad (8)$$

Based on the significant wave period, which is calculated from the significant wave height by Eq. (9), the true value of the mean wave period is obtained by Eq. (10).

$$\frac{gT_s}{2\pi U_{10}} = 3.31 \cdot \left(\frac{gH_s}{U_{10}^2}\right)^{\frac{3}{5}}, \quad (9)$$

$$T_m = 0.74 T_s\ . \quad (10)$$

The relationship between the true value of the mean wave period and significant wave height is derived as follows:

$$T_m = \frac{2\pi U_{10}}{g} \cdot 2.45 \cdot \left(\frac{gH_s}{U_{10}^2}\right)^{\frac{3}{5}}, \quad (11)$$

where T_m represents the mean wave period. The mean wave period is the upper transzero wave period calculated from the 0th-order moment and 2nd-order moment by Eq. (12) (Wang *et al.*, 2012):

$$T_m = 2\pi\sqrt{\frac{m_0}{m_2}} = 2\pi\sqrt{\frac{\int_0^\infty \int_0^\infty S\left(k_x, k_y\right) \mathrm{d}k_x \mathrm{d}k_y}{\int_0^\infty \int_0^\infty g\sqrt{k_x^2 + k_y^2} \cdot S\left(k_x, k_y\right) \mathrm{d}k_x \mathrm{d}k_y}}\ . \quad (12)$$

In this paper, the cutoff wavelength is calculated by using the spectral integration method with the Eq. (13):

$$\lambda_c = \pi\beta\sqrt{\int \left|T_k^v\right|^2 F(k) \mathrm{d}k}\ , \quad (13)$$

where $F(k)$ denotes the wavenumber spectrum, and T_k^v denotes the range-oriented velocity modulation transfer function, which is defined as follows:

$$T_k^v = -\omega\left(\sin\theta \frac{k_r}{|\boldsymbol{k}|} + \mathrm{i}\cos\theta\right), \quad (14)$$

where θ is the SAR beam incidence angle, k_r is the component of the wavenumber matrix $\boldsymbol{k}$ in the distance direction, and k_r satisfies the following relationship with k:

$$\varphi_0 = \arccos\frac{k_r}{|\boldsymbol{k}|}, \tag{15}$$

where φ_0 is the angle between the wave propagation direction and range direction of SAR.

The comparison of the inversion parameters before and after the fusion of SAR wave spectral data, as indicated in Table 1, shows that the azimuth cutoff wavelength after the fusion is reduced by 16.40%; the biases between the inversion significant wave heights and the input significant wave height before and after fusion are 0.14 m and 0.10 m, respectively. The biases between the inversion mean wave periods and the input mean wave period before and after fusion are 0.95 s and 0.78 s, respectively. These data show that the effect of azimuth cutoff is significantly reduced after wave spectrum fusion, and the errors of the effective wave height and mean wave period after fusion are smaller than those before, which validates the effectiveness of the cutoff wavelength compensation method based on the wave spectrum information fusion used in this paper.

Table 1 Comparison of wave parameters before and after the fusion of SAR wave spectrum data for the azimuth angle combination of 35°, 45°, and 55°

Optimum wave spectrum	Cutoff wavelength (m)	Significant wave height (m)		Mean wave period (s)	
		Input value	Inversion result	Input value	Inversion result
SAR1 (35°)	162.78	2.27	2.41	6.35	5.40
SAR2 (45°)	164.48	2.27	2.41	6.35	5.40
SAR3 (55°)	166.16	2.27	2.41	6.35	5.40
After data fusion	137.49	2.27	2.17	6.35	5.57

3.2 Validation for Multiview Equivalent Real Data Based on Sentinel-1 Virtual Networking

To further illustrate the effectiveness of the cutoff wavelength compensation method, it is necessary to validate the method based on the measured data. Since the SAR satellites currently in orbit do not have access to simultaneous multiview wave observation data, the azimuth cutoff wavelength compensation method cannot be directly validated using the available satellite data. To solve this problem, this paper designs and implements a validation scheme for the cutoff wavelength compensation method based on the equivalent multiview measured data obtained from the Sentinel-1 virtual networking.

Multiple observation data of one SAR satellite for the same location, at different times, under similar sea states, but for different wave propagation directions are regarded as equivalent multiview synchronous observation data. These data are used to filter and construct the equivalent synchronous data in the case of a three-satellite network, and the compensation effect of the cutoff wavelength compensation method is verified.

Three sets of SAR data with SLC (Single Look Complex) data and VV polarization methods are selected to construct the equivalent synchronized data with acquisition times of 2019/06/15 11:45:20, 2019/06/27 11:45:21 and 2019/07/09 11:45:22, latitude and longitude ranges of 12.92°–13.93°N, 93.95°–94.86°E, and the resolution of 1.49 m and 3.65 m in the range and azimuth directions, respectively. The wave spectrum fusion results are shown in Fig.4.

According to the results presented in Table 2, the cutoff wavelength decreases by 14.00% after fusion, the biases of the significant wave height and mean wave period decrease 0.14 m and 0.22 s after the compensation, respectively, and the effectiveness of the cutoff wavelength compensation method is verified by the measured SAR data.

3.3 Validation for the Buoy Data Based on the Sentinel-1 Equivalent Measurement Data

The wave parameters in the equivalent measurement data verification described in the previous subsection are derived from the calculation results of the wind speed, and the certain deviations from the actual wave parameters can be observed. The wave parameters obtained by buoys are recognized as the most accurate and can be used as the true values to verify the inversion results. Therefore, as described in this section, buoy data are used to validate the inversion results based on the Sentinel-1 equivalent data and the effectiveness of the cutoff wavelength compensation method is further illustrated.

The validation scheme is based on three buoys with three sets of wind speeds averaging 9.02 m s^{-1}, significant wave heights averaging 1.47 m, and wave directions of 308.60°, 298.00°, and 313.86°. The SAR data of the buoy locations, corresponding to the angles between the buoy wave directions and SAR track directions of 322°, 311°, and 327°, are matched. The dates are 20200226, 20200421, and 20200726, and the corresponding inversion significant wave heights of SAR data matched by buoy data are 1.92 m, 1.86 m, and 1.96 m, with inversion average wave periods of 5.04 s, 5.10 s, and 5.15 s, respectively.

The SAR subimage of 128 × 128 pixels around the location of buoys is selected. The Fourier transform of the SAR image is implemented to generate the observed SAR spectrum, and the optimal wave spectrum and optimal SAR spectrum are obtained *via* the inversion with the wind speed and wind direction by inputting E spectrum of the buoy as the first guess spectrum. As an example, the results of the wave spectrum inversion for the one-view SAR data on 20200726 are shown in Fig.5. The location and information of the SAR data matching the selected buoy data are shown in Fig.6.

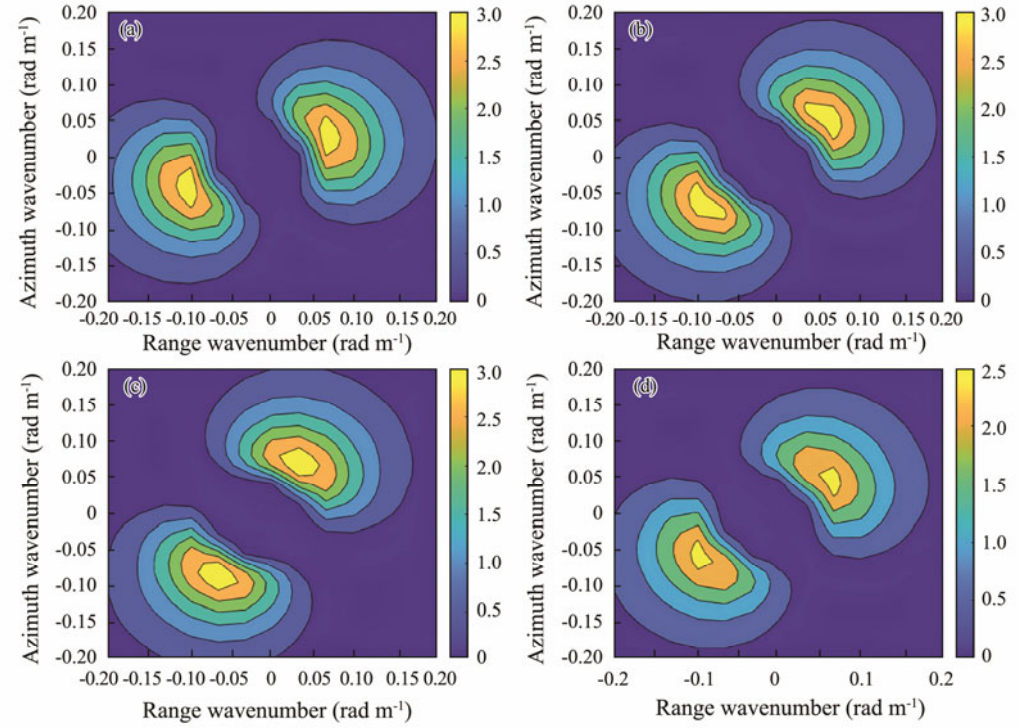

Fig.4 Results of wave spectra corresponding to different dates before and after fusion. (a), 20190615; (b), 20190627; (c), 20190709; (d), fusion of the wave spectrum.

Table 2 Comparison of wave parameters before and after the fusion of SAR wave spectrum data for different dates

Optimum wave spectrum	Cutoff wavelength (m)	Significant wave height (m)		Mean wave period (s)	
		Input value	Inversion result	Input value	Inversion result
SAR1 (20190615)	182.77	1.40	1.64	5.15	4.25
SAR2 (20190627)	177.92	1.40	1.64	5.15	4.25
SAR3 (20190709)	178.38	1.40	1.64	5.15	4.25
After data fusion	154.54	1.40	1.50	5.15	4.47

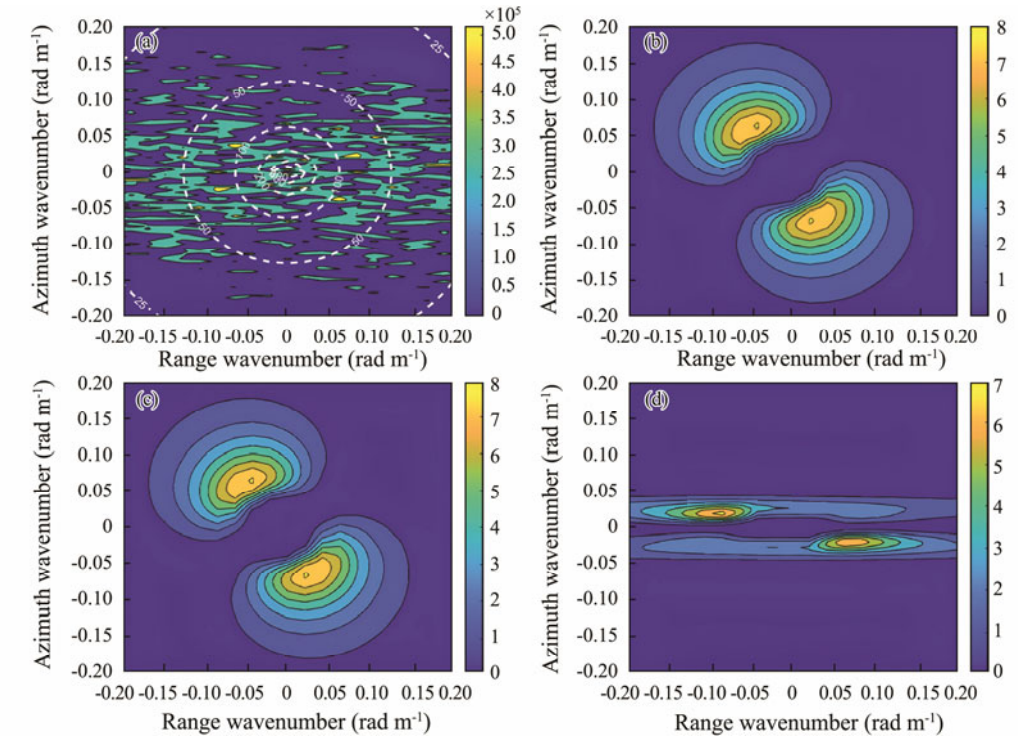

Fig.5 Results of wave spectrum inversion for SAR subimages dated 20200726.

Fig.6 The SAR image matching the buoy data. 1, 20200226; 2, 20200421; 3, 20200726.

According to the established compensation method for the cutoff wavelength, the azimuth angles of the three datasets are 322°, 311°, and 327°, and the sum of the azimuths is 960°. The azimuth angles are converted to the corresponding acute angles of 38°, 49°, and 33°, and the fusion weights are set as the ratio of each azimuth to 180°. The fusion equation is given as Eq. (16):

$$WS = \frac{38}{180}WS_1 + \frac{49}{180}WS_2 + \frac{33}{180}WS_3, \qquad (16)$$

where WS_1, WS_2 and WS_3 represent the SAR wave spectra of each satellite and WS is the wave spectrum after fusion. The results of fusion are shown in Fig.7.

The comparisons of the inverse wave parameters and buoy wave parameters before and after the cutoff wavelength compensation are shown in Table 3. The results indicate that the cutoff wavelength decreases by 19.62% after fusion, the biases of significant wave height and mean wave period decreases by 0.36 m and 0.04 s after compensation, respectively; the root mean square error of significant wave height is 0.08 m, the root mean square error of mean wave period is 0.26 s. The inversion accuracy of wave parameters after multisatellite network compensation is better than that of single-satellite inversion, and the effectiveness of the cutoff wavelength compensation method is verified by the measured SAR data and buoy data.

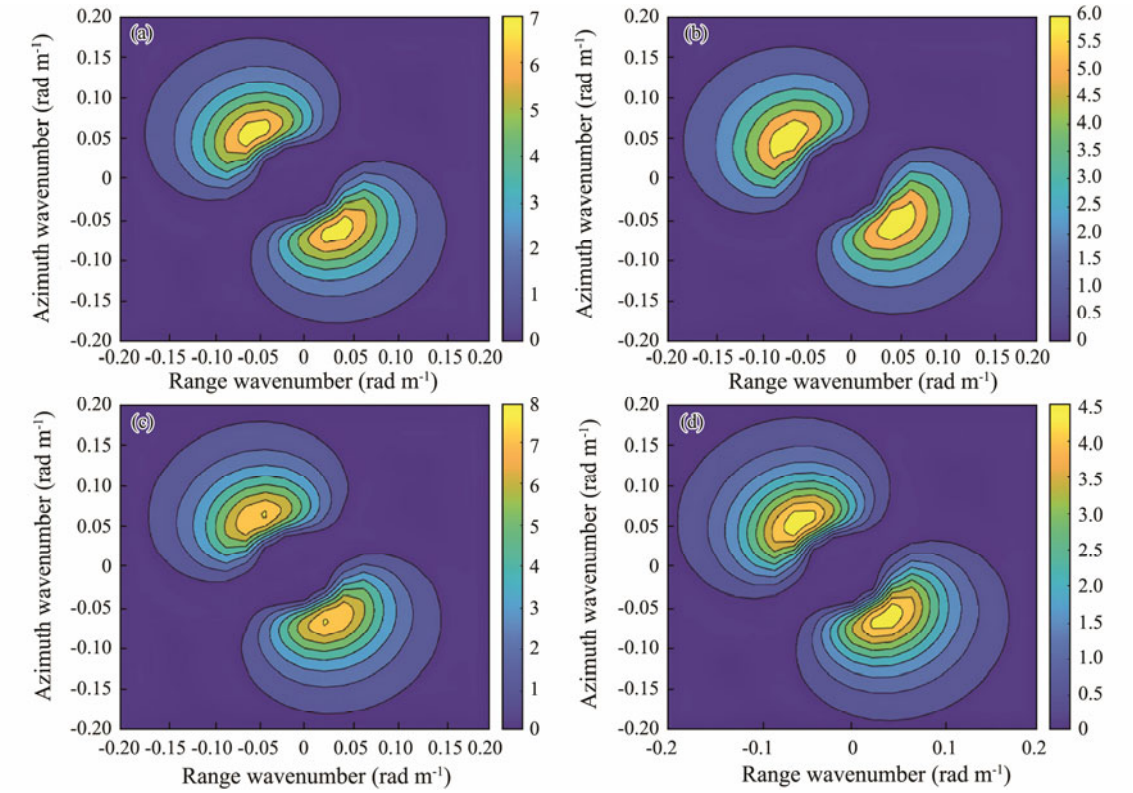

Fig.7 Results of wave spectra corresponding to different dates before and after fusion.

3.4 Validation of Cutoff Wavelength Compensation for Equivalent Multiview Data Based on Buoy Data

To further verify the compensation effect by using the equivalent measurement data, we use the wind speed and wind direction information obtained by the buoy as the input to construct the simulated equivalent measurement data, and then processes the data by the established cutoff wavelength compensation method. The wave parameters

Table 3 Comparison of inverse wave parameters and buoy wave parameters before and after cutoff wavelength compensation

Optimum wave spectrum	Cutoff wavelength (m)	Significant wave height (m)		Mean wave period (s)	
		Buoy value	Inversion result	Buoy value	Inversion result
SAR1 (20190226)	209.88	1.47	1.92	5.40	5.04
SAR2 (20190421)	193.05	1.47	1.86	5.40	5.10
SAR3 (20190726)	209.77	1.47	1.96	5.40	5.15
After data fusion	164.17	1.47	1.55	5.40	5.14

calculated after compensation are compared with those of the buoy to verify the effect of the compensation method.

The validation scheme is performed on the NDBC buoy data with the observation date of 20200329, time of 01:40:00, latitude of 32.404°N, longitude of 119.506°W, wind speed of 9.1 m s^{-1}, wind direction of 322°, significant wave height of 1.80 m, and mean wave period of 5.40 s.

The simulated sea surface and simulated backscatter coefficients are established according to the wind speed and wind information from the buoy, and then the simulated echo and SAR images are obtained. The sea surface is rotated by 10° and 20° respectively to obtain the simulated SAR images with 10° and 20° rotation, as shown in Fig.8. The simulated multiview SAR data are processed by the established cutoff wavelength compensation technique, and the inversion results after compensation are compared with the buoy data, as shown in Table 4. The results show that the cutoff wavelength decreases significantly after the wave spectrum fusion, and the inversion results of significant wave height and mean wave period are closer to the measured values of buoy. The inversion accuracy of wave parameters after the multisatellite network compensation is

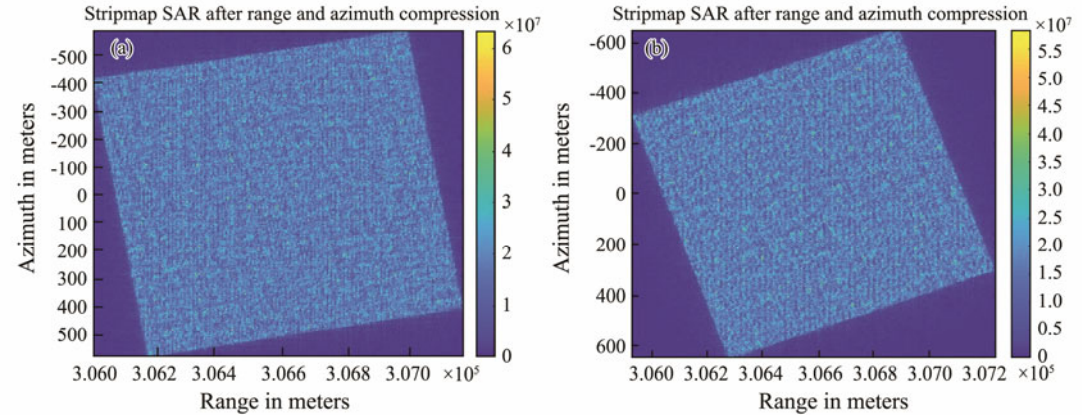

Fig.8 SAR image results for different wind directions. (a), 312°; (b), 302°.

Table 4 Validation results of cutoff wavelength compensation method for the simulated data based on buoy data

Optimum wave spectrum	Cutoff wavelength (m)	Significant wave height (m)		Mean wave period (s)	
		Buoy value	Inversion result	Buoy value	Inversion result
SAR1	148.11	1.81	2.02	5.37	5.01
SAR2	149.69	1.81	2.02	5.37	5.01
SAR3	151.19	1.81	2.02	5.37	5.01
After data fusion	128.27	1.81	1.79	5.37	5.19

better than that of the single satellite, with the root mean square errors of significant wave height and mean wave period of 0.02 m and 0.18 s respectively, which verifies the effectiveness of cutoff wavelength compensation technique.

4 Optimal Networking Mode of Small Satellite SARs for Wave Observation

We analyze the compensation effect of the cutoff wavelength based on the simulated multiview synchronization SAR wave data with different combinations of orbital crossing angles and different azimuth angles at a wind speed of 10 m s^{-1}. The optimal combination of the orbital crossing angles and the optimal azimuth angle in view of the highest compensation effect and the optimal satellite networking mode with different number of satellites are determined.

4.1 Optimal Networking Mode with Different Combinations of Orbital Intersection Angles

Table 5 lists the results of cutoff wavelength compensation and parameter inversion for different combinations of orbital intersection angles. For each group of orbital intersection angles, all the azimuth angle combinations are involved.

The inversion significant wave height of the first guess wave spectrum and average wave period are 2.41 m, and

Table 5 Cutoff wavelength compensation effect and parameter inversion results for different combinations of orbital intersection angles

Orbital intersection angle combination (˚)	Average cutoff wavelength after fusion (m)	Average percentage reduction in the cutoff wavelength	Significant wave height of the inversion after fusion (m)	Mean wave period of the inversion after fusion (m)	RMSE of the inversion significant wave height after fusion	RMSE of the inversion mean wave period after fusion
10, 10	142.14	14.30%	2.12	5.57	0.3455	0.1641
20, 20	143.23	13.41%	2.13	5.56	0.3177	0.1515
30, 30	138.96	15.79%	2.05	5.54	0.3865	0.1368
40, 40	148.11	10.14%	2.18	5.54	0.2496	0.1358
50, 50	148.18	10.31%	2.19	5.54	0.2391	0.1331
60, 60	142.26	13.49%	2.11	5.53	0.3059	0.1271

5.40 s, respectively, which are considered as the input values. After data fusion and cutoff wavelength compensation for the multisatellite simultaneous data under different orbital cross-angle combinations, the cutoff wavelengths exhibit different degrees of degradation. In terms of the inversion accuracy of the significant wave height and mean wave period, the (50˚, 50˚) orbit intersection angle combination get the highest values and is selected as the optimal combination. As an example, the wave spectrum results for the azimuth angle combination (5˚, 55˚, 105˚) are shown in Fig.9.

4.2 Optimal Networking Mode with Different Combinations of Azimuth Angles

For a given orbital intersection angle combination, the inversions with different combinations of azimuth angles exhibit different degrees of decrease in the cutoff wavelength after fusion. Therefore, six azimuth angle combinations are screened for different orbital intersection angles from (10˚, 10˚) to (60˚, 60˚) at an interval of 10˚ to determine the optimal azimuth angle combination with the highest compensation effect. The results are shown in Table 6.

The inversion results of the significant wave height of the first guess wave spectrum and mean wave period are 2.41 m and 5.40 s, respectively, which are considered as the input values. According to the inversion results, the highest accuracy is obtained for the azimuth angle combination (95˚, 115˚, 135˚) with the combination of orbital intersection angle (20˚, 20˚).

4.3 Optimal Networking Mode with Different Numbers of Satellites

The effect of the cutoff wavelength compensation technique is analyzed and verified when different numbers of

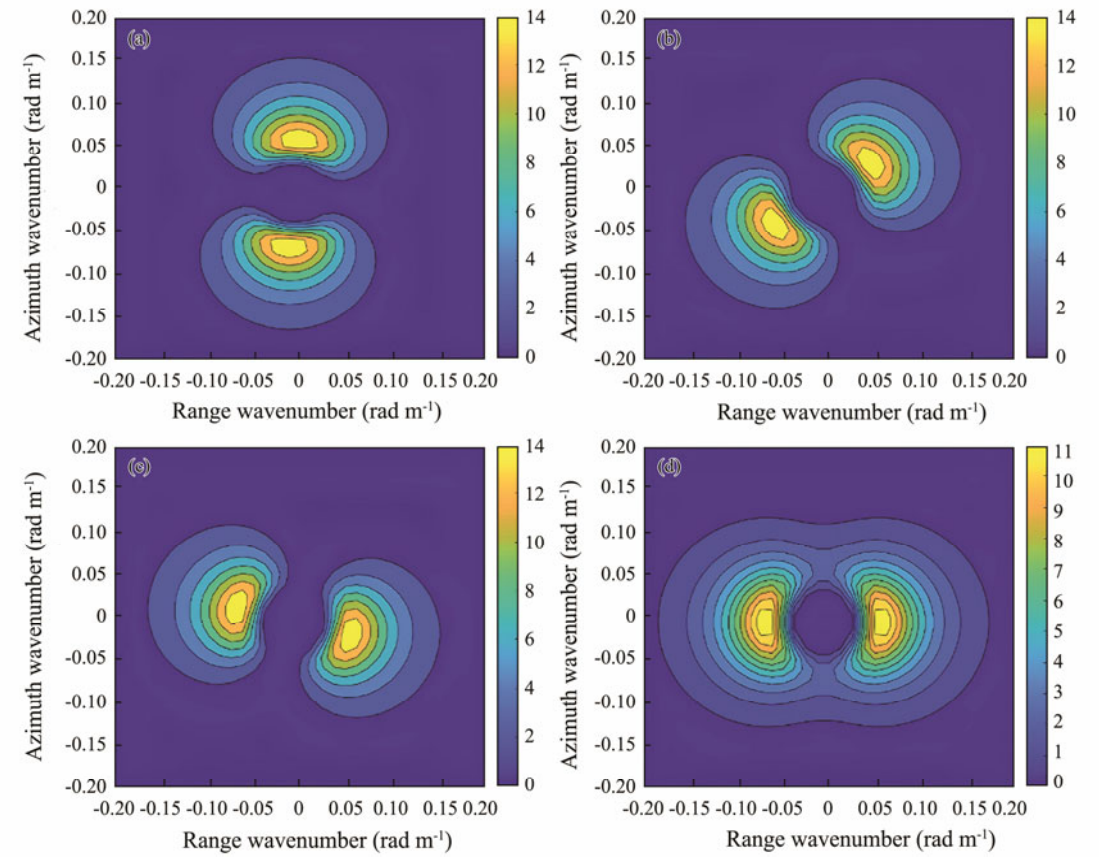

Fig.9 Results of wave spectra for combinations of azimuths (5˚, 55˚, 105˚). (a), 5˚; (b), 55˚; (c), 105˚; (d), fusion of the wave spectrum.

Table 6 Optimal combination of azimuth angles for six orbital intersection angles

Azimuth angle combination (°)	Cutoff wavelength of SAR1 (m)	Cutoff wavelength of SAR2 (m)	Cutoff wavelength of SAR3 (m)	Cutoff wavelength after fusion (m)	Significant wave height of the inversion after fusion (m)	Mean wave period of the inversion after fusion (m)
105, 115, 125	168.71	167.63	166.16	158.12	2.34	5.57
95, 115, 135	169.28	167.63	164.48	158.29	2.34	5.56
25, 55, 85	161.27	166.16	169.28	154.81	2.29	5.55
15, 55, 95	160.14	166.16	169.28	155.37	2.29	5.55
35, 85, 135	162.78	169.28	164.48	156.22	2.32	5.55
15, 75, 135	160.14	168.71	164.48	146.80	2.18	5.54

satellites are used for observation, and the optimal number is determined. As an example, two sets of networking mode with different azimuth angle combinations for a given number of satellites are considered. The effects of the cutoff wavelength compensation and parameter inversion results are shown in Tables 7 and 8.

The inversion results of the significant wave height of the first guess wave spectrum and mean wave period are 2.41 m and 5.40 s, respectively. A larger number of satellites corresponds to a superior effect after fusion compensation; however, the system cost increases as well, and the time resolution of the same area observed by multiple satellites decreases. Therefore, in view of the cost and time resolution, the number of satellites should not be too large, and three or four satellites can be used to obtain the acceptably high cutoff wavelength compensation effect.

Table 7 Effect of cutoff wavelength compensation under the networking modes with different numbers of satellites

Number of satellite	Azimuth angle combination (°)	Cutoff wavelength of SAR1 (m)	Cutoff wavelength of SAR2 (m)	Cutoff wavelength of SAR3 (m)	Cutoff wavelength of SAR4 (m)	Cutoff wavelength of SAR5 (m)	Cutoff wavelength after fusion (m)
2	45, 55	158.56	159.96	–	–	–	125.08
	75, 85	160.99	161.54	–	–	–	146.34
3	25, 35, 45	161.27	162.78	164.48	–	–	120.14
	55, 65, 75	166.16	167.63	168.71	–	–	137.45
4	45, 55, 65, 75	158.56	159.96	160.99	161.54	–	152.56
	95, 105, 115, 125	161.54	160.99	159.96	158.56	–	144.51
5	45, 55, 65, 75, 85	156.95	158.56	159.96	160.99	161.54	146.16
	95, 105, 115, 125, 135	161.54	160.99	159.96	158.56	156.95	146.83

Table 8 Parameter inversion results under networking modes with different numbers of satellites

Number of satellite	Azimuth angle combination (°)	Significant wave height (m)		Mean wave period (s)	
		Input value	Inversion result	Input value	Inversion result
SAR1	45, 55	2.41	1.95	5.40	5.58
	75, 85	2.41	2.25	5.40	5.58
SAR2	25, 35, 45	2.41	1.82	5.40	5.57
	55, 65, 75	2.41	2.03	5.40	5.57
SAR3	45, 55, 65, 75	2.41	2.36	5.40	5.58
	95, 105, 115, 125	2.41	2.25	5.40	5.58
After data fusion	45, 55, 65, 75, 85	2.41	2.26	5.40	5.58
	95, 105, 115, 125, 135	2.41	2.28	5.40	5.58

5 Conclusions

This paper analyzes the cutoff wavelength compensation method based on the simulated multiview SAR wave synchronization data, verifies the effectiveness of the cutoff wavelength compensation method through simulated and measured data, and finally examines the multisatellite SAR networking mode for wave observations based on this cutoff wavelength compensation method. The following conclusions are drawn.

1) The compensation effect of the cutoff wavelength compensation method is verified using the simulated data and equivalent multiview measured data based on the Sentinel-1 virtual networking. The cutoff wavelength decreases by 16.40% and 14.00%, the biases of the significant wave height decrease by 0.04 m and 0.14 m, and the biases of the mean wave period decrease by 0.17 s and 0.22 s, respectively. The significant wave height and mean wave period obtained by the inversion after cutoff wavelength compensation approach the true values. Therefore, the proposed cutoff wavelength compensation method is effective.

2) Considering the inversion accuracy, cost and other aspects, the optimal number of satellites is determined to be three or four, the optimal combination of the satellite orbit intersection angles is (50°, 50°), and the azimuth angle of (95°, 115°, 135°) with the orbit intersection angles of (20°, 20°) represents the optimal combination.

The optimal multisatellite networking mode is determined for different orbital intersection angles, azimuth angles and numbers of satellites, which can provide valuable reference for the design of future multisatellite networking observation modes, compensation of cutoff wavelength by multisatellite network technology and wave observation by SAR satellite networks. Moreover, these works can promote the operational application of SAR in the

wave observation.

Acknowledgements

The authors acknowledge the support of the National Natural Science Foundation of China (No. 61931025), and the National Key R&D Program of China (No. 2017YFC 1405600).

References

Alpers, W., 1985. Theory of radar imaging of internal waves. *Nature*, **314** (6008): 245-247, DOI: 10.1038/314245a0.

Bruck, M., and Lehner, S., 2012. Sea state measurements using TerraSAR-X data. *IEEE International Geoscience and Remote Sensing Symposium*, **8536**: 7609-7612, DOI: 10.1109/igarss.2012.6351866.

Corcione, V., Grieco, G., Portabella, M., Nunziata, F., and Migliaccio, M., 2018. A novel azimuth cutoff implementation to retrieve sea surface wind speed from SAR imagery. *IEEE Transactions on Geoscience and Remote Sensing*, **57** (6): 3331-3340, DOI: 10.1109/TGRS.2018.2883364.

Engen, G., and Johnsen, H., 1995. SAR-ocean wave inversion using image cross spectra. *IEEE Transactions on Geoscience and Remote Sensing*, **33** (4): 1047-1056, DOI: 10.1109/36.406690.

Grieco, G., Lin, W., Migliaccio, M., Nirchio, F., and Portabella, M., 2016. Dependency of the Sentinel-1 azimuth wavelength cut-off on significant wave height and wind speed. *International Journal of Remote Sensing*, **37** (21): 5086-5104.

Guo, D., 2011. SAR imaging simulations based on the ocean scenes and the electromagnetic scattering study. Master thesis. University of Electronic Science and Technology (in Chinese).

Hasselmann, K., and Hasselmann, S., 1991. On the nonlinear mapping of an ocean wave spectrum into a synthetic aperture radar image spectrum and its inversion. *Journal of Geophysical Research: Oceans*, **96** (C6): 10713, DOI: 10.1029/91jc00302.

Hasselmann, K., Raney, R. K., Plant, W. J., Alpers, W., Shuchman, R. A., Lyzenga, D. R., *et al*., 1985. Theory of synthetic aperture radar ocean imaging: A MARSEN view. *Journal of Geophysical Research: Oceans*, **90** (C3): 4659-4686, DOI: 10.1029/jc090ic03p04659.

He, Y. J., 1999. A parametric method for extracting wave direction spectrum by synthetic aperture radar. *Science Bulletin*, **44** (4): 428-433.

He, Y. J., Perrie, W., Xie, T., and Zou, Q. P., 2004. Ocean wave spectra from a linear polarimetric SAR. *IEEE Transactions on Geoscience and Remote Sensing*, **42** (11): 2623-2631, DOI: 10.1109/tgrs.2004.836813.

Huang, Y. K., 2008. Modeling simulation and system design of synthetic aperture radar echo simulator. Master thesis. University of Electronic Science and Technology (in Chinese).

Kerbaol, V., Chapron, B., Fouhaily, T. E., and Garello, R., 1996. Fetch and wind dependence of SAR azimuth cutoff and higher order statistics in a mistral wind case. *IGARSS'96. 1996 International Geoscience and Remote Sensing Symposium*. Lincoln, 621-624, DOI: 10.1109/igarss.1996.516422.

Li, H. M., Mouche, A., Wang, H., Stopa, J. E., and Chapron, B., 2019. Polarization dependence of azimuth cutoff from quadpol SAR images. *IEEE Transactions on Geoscience and Remote Sensing*, **57** (12): 9878-9887, DOI: 10.1109/tgrs.2019.2929835.

Li, X. M., 2010. Research on wave inversion algorithm for ASAR wave pattern data from ENVISAT satellite. Master thesis. Ocean University of China (in Chinese).

Lin, B., Shao, W. Z., Li, X. F., Li, H., Du, X. Q., Ji, Q. Y., *et al*., 2017. Development and validation of an ocean wave retrieval algorithm for VV-polarization Sentinel-1 SAR data. *Acta Oceanologica Sinica*, **36** (7): 95-101, DOI: 10.1007/s13131-017-1089-9.

Lyzenga, D. R., and Malinas, N. P., 1996. Azimuth falloff effects in two-antenna SAR measurements of ocean wave spectra. *IEEE Transactions on Geoscience and Remote Sensing*, **34** (4): 1020-1028, DOI: 10.1109/36.508419.

Mao, C., Qiu, Z. M., Liu, Z., and Lu, F., 2013. Monte Carlo simulation of three-dimensional random rough sea surface. *Ship Science and Technology*, **35**: 25-28 (in Chinese with English abstract).

Marghany, M., Ibrahim, Z., and Genderen, J. V., 2002. Azimuth cut-off model for significant wave height investigation along coastal water of Kuala Terengganu, Malaysia. *International Journal of Applied Earth Observation and Geoinformation*, **4** (2): 147-160.

Mastenbroek, C., and de Valk, C. F., 2000. A semiparametric algorithm to retrieve ocean wave spectra from synthetic aperture radar. *Journal of Geophysical Research: Oceans*, **105** (C2): 3497-3516, DOI: 10.1029/1999jc900282.

Pi, Y. M., Yang, J. Y., Fu, Y. S., and Yang, X. B., 2007. *Synthetic Aperture Radar Imaging Principle*. University of Electronic Science and Technology of China Press, Sichuan, 78-82.

Ren, L., Yang, J. S., Zheng, G., and Wang, J., 2015. Significant wave height estimation using azimuth cutoff of C-band RADARSAT-2 single-polarization SAR images. *Acta Oceanologica Sinica*, **34** (12): 93-101, DOI: 10.1007/s13131-015-0769-6.

Ren, L., Yang, J. S., Zheng, G., and Wang, J., 2016. A joint method to retrieve directional ocean wave spectra from SAR and wave spectrometer data. *Chinese Journal of Oceanology and Limnology*, **34** (4): 847-858, DOI: 10.1007/s00343-015-5043-4.

Romeiser, R., Graber, H. C., Caruso, M. J., Jensen, R. E., Walker, D. T., and Cox, A. T., 2015. A new approach to ocean wave parameter estimates from C-band ScanSAR images. *IEEE Transactions on Geoscience and Remote Sensing*, **53** (3): 1320-1345, DOI: 10.1109/tgrs.2014.2337663.

Schuler, D. L., Lee, J. S., Kasilingam, D., and Pottier, E., 2004. Measurement of ocean surface slopes and wave spectra using polarimetric SAR image data. *Remote Sensing of Environment*, **91** (2): 198-211, DOI: 10.1016/S0034-4257(04)00078-1.

Schulz-Stellenfleth, J., Lehner, S., and Hoja, D., 2005. A parametric scheme for the retrieval of two-dimensional ocean wave spectra from synthetic aperture radar look cross spectra. *Journal of Geophysical Research: Oceans*, **110**: C05004, DOI: 10.1029/2004jc002822.

Stopa, J. E., Ardhuin, F., Chapron, B., and Collard, F., 2015. Estimating wave orbital velocity through the azimuth cutoff from space-borne satellites. *Journal of Geophysical Research: Oceans*, **120** (11): 7616-7634, DOI: 10.1002/2015JC011275.

Sun, J., 2005. Inversion of wave information from SAR images. Master thesis. Ocean University of China (in Chinese).

Vachon, P., Krogstad, H., and Scottpaterson, J., 1994. Airborne and spaceborne synthetic aperture radar observations of ocean waves. *Atmosphere*, **32** (1): 83-112, DOI: 10.1080/07055900.1994.9649491.

Wan, Y., Zhang, X. Y., Dai, Y. S., and Shi, X. L., 2019. Research on a method for simulating multiview ocean wave synchronization data by networked SAR satellites. *Journal of Marine Science and Engineering*, **7** (6): 180, DOI: 10.33 90/jmse7060180.

Wan, Y., Zhang, X. Y., Dai, Y. S., and Shi, X. L., 2020a. An azimuth cut-off wavelength compensation method based on multiview synthetic aperture radar synchronization data. *Remote Sensing Letters*, **11** (3): 245-254, DOI: 10.1080/2150704X.2019.1706008.

Wan, Y., Zhang, X. Y., Dai, Y. S., Li, L. G., and Qu, X. J., 2020b. Azimuth cutoff compensation method for SAR wave observation based on multiview wave spectrum data fusion. *IEEE Access*, **8**: 120923-120935, DOI: 10.1109/access.2020.3006244.

Wang, H., Zhu, J. H., and Yang, J. S., 2012. A semiempirical algorithm for SAR wave height retrieval and its validation using Envisat ASAR wave mode data. *Acta Oceanologica Sinica*, **31** (3): 59-66, DOI: 10.1007/s13131-012-0206-z.

Xu, X. J., Li, X. F., Diao, G. J., and Jiang, D., 2013. *Radar Phenomenological Models for Ships on Time-Evolving Sea Surface*. National Defense Industry Press, Beijing, 29-30.

Zhang, Z., 2017. Research on the extraction of sea surface wind and wave parameters by synthetic aperture radar. Master thesis. Zhejiang Ocean University (in Chinese).

Zheng, C. W., Zhang, G., Chen, Y. G., Wang, X. L., Xiao, Z. N., and Li, D. L., 2020. Establishment of wave climate datasets: Case study for the Maritime Silk Road. *2020 6th International Conference on Big Data and Information Analytics (BigDIA)*. Shenzhen, 451-456, DOI: 10.1109/BigDIA51454.2020.00080.

(Edited by Chen Wenwen)